



## Application of alumina/graphene nanocomposite to enhance the surface quality of Al7175-T74 specimens

S. Khalilpourazary<sup>1,\*</sup>, S.S. Meshkat<sup>2</sup>, J. Salehi<sup>1</sup>

<sup>1</sup> Faculty of Mechanical Engineering, Urmia University of Technology, Urmia, Iran

<sup>2</sup> Faculty of Chemical Engineering, Urmia University of Technology, Urmia, Iran

**ABSTRACT:** The burnishing process is one of the non-removal finishing processes, which is employed to enhance surface quality, corrosion property, and surface microhardness. In this study, the dry burnishing process was performed on the surface of Al7175-T74 specimens. Furthermore, nanofluid containing alumina/graphene nanocomposite was employed to perform the Nano burnishing process on the same specimens. The results show that the arithmetic surface roughness parameter in nanofluid burnished samples is decreased by approximately 0.277  $\mu\text{m}$ , 0.233  $\mu\text{m}$ , and 0.345  $\mu\text{m}$  for the penetration depths of 0.2, 0.3, and 0.4mm compared to those of dry burnishing process. Moreover, microhardness values in Nano and dry burnishing processes are directly related to the penetration depth parameter. The results reveal that the values of microhardness for the nanofluid burnished samples with four penetration depths of 0.2, 0.3, 0.4, and 0.5 mm are increased about 3, 28, 42, and 39 Vickers comparing to those values of the dry burnishing process. The results prove that the minimum surface roughness and maximum microhardness values can be reached in Nano and dry roller burnishing processes at the penetration depth of 0.4 mm. Eventually, analyzing elements distribution on the surface of burnished aluminum alloy specimens confirm that the alumina/graphene nanocomposite is embedded in the burnished surfaces during Nano burnishing process.

### Review History:

Received: Nov. 24, 2019

Revised: May, 07, 2020

Accepted: Aug. 31, 2020

Available Online: Sep. 02, 2020

### Keywords:

Roller burnishing

Alumina

Graphene

Nanofluid

Surface characteristics

### 1- Introduction

Sequential finishing operations, such as grinding process, are employed to improve the surface quality and overcome the design requirements of the specimens manufactured through conventional machining processes. The finishing process as a subtractive process not only removes the materials in the chip form but also requires extra expenses to purchase a new precision machine tool which increases the cost of products [1]. Furthermore, the finishing process is of greater importance in lightweight metals such as aluminum due to their wide applications in various industries. The burnishing process is one of the non-removal machining processes, which is utilized to enhance surface quality, corrosion property, wear resistance, and surface resistance against fatigue [2]. In this method, there is no chip produced throughout the process; also there is almost no need to use lubricant and coolant [3-5]. In the burnishing process the applied tool pressure which is greater than the yield strength limit of the material results in cold plastic deformation on its surface. In other words, the combination of burnishing tool pressure and machine feed rate along with burnished length decreases the height of surface peaks which in turn fills the valleys on the surface in microscale. Previous studies have proved that the surface microhardness increases after burnishing process due to

plastic deformation. The surface microhardness has a direct relationship with the number of passes and the force applied to the workpiece surface during the burnishing process [6-8]. To promote the performance of the burnishing process, a great deal of research has aimed at studying the factors effective on it. The impressive parameters on the burnishing process can be divided into i) the characteristics of the burnishing tool, ii) using or not using lubricant and coolant during the process, iii) burnishing parameters such as speed, depth of penetration, and the number of passes and iv) the workpiece material.

### 2- A Survey on Research Conducted

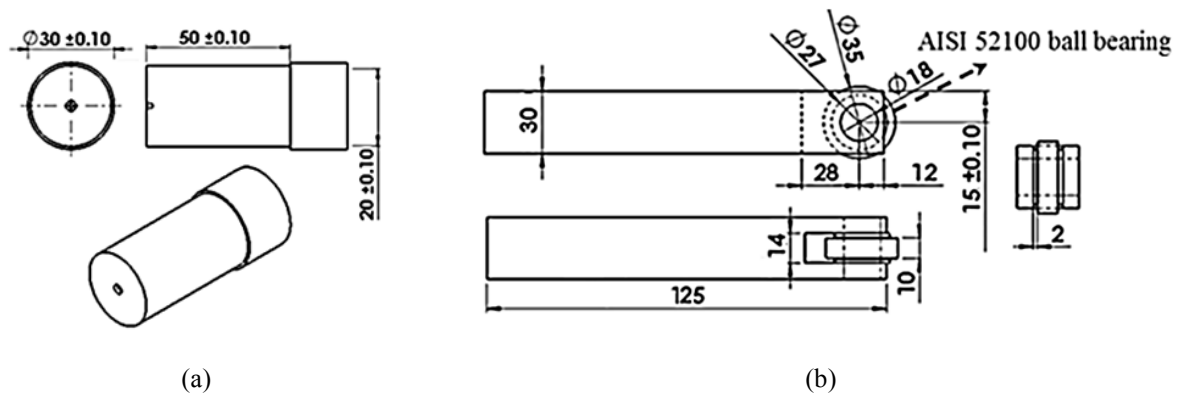
Sachin et al. have studied the effect of Minimum Quantity Lubrication (MQL) in the diamond burnishing process of stainless steel [9]. The results declared that the suggested burnishing tool has a significant effect to enhance the surface quality and surface hardness under MQL condition. Also, Sachin et al. experimentally investigated the influence of the cryogenic diamond burnishing process on the surface quality and residual stress of 17-4 pH stainless steel [10]. The results revealed that the surface quality/microhardness values are generally more decreased/increased in the suggested burnishing process compared with MQL and dry burnishing processes. Ebeid and Ei-Taweel used a hybrid approach combining electrochemical turning and roller burnishing processes to achieve minimum surface roughness

\*Corresponding author's email: saman\_azari@yahoo.com



**Table 1. Chemical composition of Al7175 at a temperature and moisture of 25 °C and 29%**

Element	Al	Mg	Zn	Pb	Sb	Cu	Si	Other
Weight (%)	89.2	2.27	5.49	0.166	0.122	1.975	0.105	0.672

**Fig. 1. Dimensions of the, a) initially machined workpieces before the burnishing process, b) burnishing tool (in mm) [14]**

and maximum material removal rate on Al-Zn-Mg alloy workpieces [11]. The optimum input parameters to gain this goal were determined via the Taguchi method. Luo et al. evaluated the effect of burnishing parameters such as feed rate, workpiece speed, and penetration depth on the burnishing force of the Al-alloy LY12 and Brass H62 in the turning process [12]. The results presented that the penetration depth has the greatest impact on the burnishing force.

Özkul studied the effect of the force, feed rate, and the number of passes on the surface quality of Al6013 in the ball burnishing process [13]. To investigate the effect of these parameters on the surface quality analysis of variance method (ANOVA) was employed. The results revealed that the high force and feed ratio directly increase the final surface quality in the ball burnishing process. Also, experiments proved that the number of passes has a minimum effect on the surface quality.

Kalilpourazary and Salehi investigated the effect of Alumina Nanoparticles (ANs) nanofluid in the roller burnishing process of Al7175 [14]. The roller burnishing process was performed in dry and nanofluid types to scrutinize the final surface quality and microhardness values of the burnished samples. The input parameters of the burnishing process were selected the same in both burnishing strategies. The results indicated the use of the alumina nanofluid significantly increases the surface quality and surface microhardness values comparing to the conventional dry burnishing process.

The effect of nanoparticles on the machining process can be studied in terms of the following concepts: i) the type/size of nanoparticles being used, ii) the effect of nanoparticles on the characteristics of machined surface such as surface

quality and microhardness, and iii) the effect of nanoparticles on the tool wear, tool life, etc. [15].

The main goal of this research is to investigate the effect of Alumina/Graphene NanoComposite (AGNC) dispersed in ethanol as a nanofluid on the surface quality and microhardness values in the roller burnishing process of Al7175.

In this study, each of the dry and AGNC burnishing processes was carried out on two separate groups of 5 samples made of Al7175-T74. The input parameters such as penetration depth, burnishing depth, number of passes, feed rate, speed, and burnishing tool were selected to be the same for all the samples in the burnishing process. To assess the effect of using AGNC in the burnishing process, the arithmetic surface roughness ( $R_a$ ), and microhardness parameters were investigated. Moreover, by using the Electron Dispersion Spectroscopy (EDS), the elements on the surface of the Al7175 specimens after performing the burnishing process were analyzed.

### 3- Materials and Methods

The initial material used in experiments is Al7175-T74. It is a common aluminum alloy in industrial applications such as automotive and aerospace industries due to its high machinability and formability. It has the highest ductility compared to the other variants of 7175 aluminum. The chemical percentages of the used Al7175-T74 are given in Table 1.

Before the burnishing, the machining process was performed on cylindrical workpieces of Al7175-T74 on Colchester Tornado CNC turning machine. A roller bearing made of AISI 52100 with high carbon and chromium content was used to perform the roller burnishing process on the CNC turning machine. Fig. 1 reflects the machined workpieces and

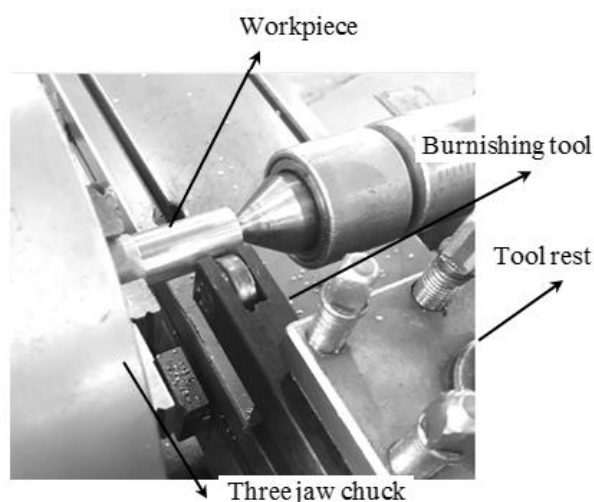


**Fig. 2. Experimental setup of the burnishing process in turning machine**

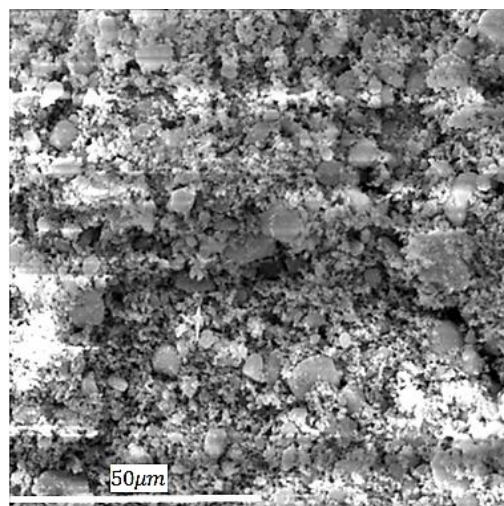


**Fig. 3. SEM image of the alumina nanoparticles**

**Table 2. Characteristics of the  $\gamma$ -Al<sub>2</sub>O<sub>3</sub> nanoparticles [14]**

Parameter	Value
Purity	99%
Color	White
Particle Average Size	50 nm
Morphology	spherical
Density	3720 kg/m <sup>3</sup>

burnishing tool drawings.

Dry burnishing process was performed for the first 5 aluminum alloy samples with fixed values of speed and feed; penetration depth values and number of passes were different from one sample to another. For all the samples, the number of spindle rotation, feed rate, and maximum depth in each longitudinal tool traverse across the workpiece in the burnishing process were selected to be 180 rev/min, 0.11 mm/rev, and 0.1 mm, respectively. Fig. 2 shows the experimental setup of the dry burnishing process with the burnishing tool and cylindrical workpiece.

Al7175-T74 contains hard silicon particles in the microstructure which can increase the tool wear rate. Many scientists showed that aluminum series 7xxx can be machined effectively at low cutting speeds and feeds [16, 17].

In the burnishing process, as the feed rate of the burnishing tool decreases, because of the long-time that the burnishing tool is in contact with the surface of specimens, the bearing stress applied to the surface increases, and obtaining high surface quality becomes possible. Rotational speed 180 rev/min is selected as an optimized value in the aluminum series 7xxx burnishing process [18].

### 3- 1- Nanofluid preparation

#### 3- 1- 1- Alumina nanoparticles

To perform the burnishing process on the second group of aluminum alloy workpieces, a nanofluid including AGNC was prepared. Alumina as a ceramic material has good physical property, high chemical stability, and hardness [19]. General information to characterize the mechanical and thermal properties of  $\gamma$ -Al<sub>2</sub>O<sub>3</sub> nanoparticles are given in Table 2. In this paper, the used alumina nanoparticles have been provided by Shanghai Xinglu Chemical Technology Co. Fig. 3 presents a Scanning Electron Microscopy (SEM) image of the ANs.

#### 3- 1- 2- Graphene

In this paper, graphene was employed as a carbon-based nanomaterial with a high surface area when mixed with alumina nanoparticles [20-22]. Graphene with a layered structure increases the lubrication property of the metal's surface and toughness [23]. Compared to the carbon nanotubes, graphene can be homogeneously distributed in a matrix. The graphene layers are related to each other with weak Van Der Waals forces, and their movement on each other improves lubrication characteristics.

The graphene nanoparticles have been synthesized by the authors of this work using the Chemical Vapor Deposition (CVD) method. In this method, methane gas (CH<sub>4</sub>) was used as a carbon source. Also, NiO nanoparticles were synthesized through Sol-gel process and were used as the Catalyst [24]. Methane gas and hydrogen with a ratio of 4:1 were utilized as the carrier gas in this method. A gas mixture was passed through the quartz tube for 30 min, and the furnace was heated up to 900-1000 °C. To acquire the pure nanoporous Graphene, the prepared graphene was stirred in acid solution (HCl) for about 16h then it was rinsed with distilled water

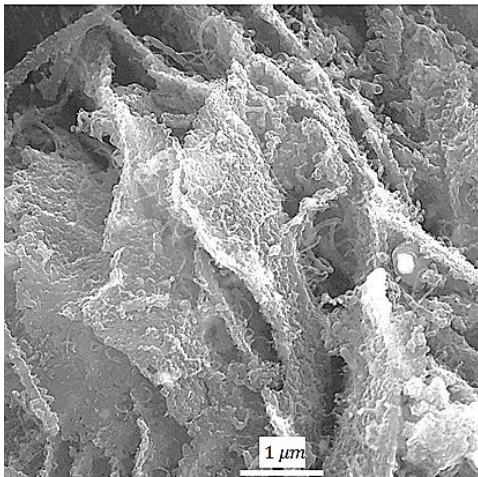


**Fig. 4.** SEM micrograph of the graphene nanoparticles

several times to achieve the neutral pH [25]. Fig. 4 represents the morphology of graphene nanoparticles with a layered structure.

### 3- 1- 3- Alumina/Graphene nanocomposite

To obtain AGNC, the  $\gamma$ - $Al_2O_3$  and 0.5wt% graphene powders were blended [26, 27]. It is shown that 0.5wt% graphene in  $\gamma$ - $Al_2O_3$  matrix increases the mechanical properties of alumina/graphene composite such as wear-resistance and hardness [28].

To synthesis AGNC, the primary compounds are blended with the mixer for 5 minutes. The powder mixtures were milled for 1 hour by Argon gas with a speed of 100rpm to reach homogenized condition. Fig. 5 reflects the accumulation of ANs inside the plate-type structure of graphene.

In this study, a carrier fluid including Ethanol alcohol ( $C_2H_5OH$ ) named nanofluid is employed to deliver AGNC to the workpiece surface in the burnishing process. Ethanol alcohol is a volatile liquid and evaporates at room temperature, and has never been utilized as a coolant and lubricant in the machining or burnishing processes. According to Eq. (1), AGNC is not soluble in Ethanol alcohol and there is no chemical reaction among Ethanol alcohol, graphene, and ANs.



To provide the uniform AGNC in an Ethanol alcohol solution, an ultrasonic bath has been used for 5 minutes. According to the hydrophobic and hydrophilic groups on the graphene surface, graphene solution in Ethanol alcohol is stable and stays uniform during the burnishing process; therefore the graphene is not agglomerated in the inorganic solutions.

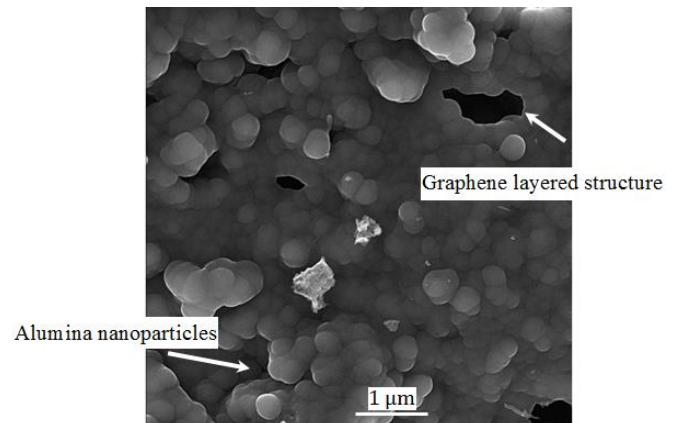


**Fig. 5.** SEM image of the alumina/graphene nanocomposite

### 3- 2- Nanofluid burnishing parameters

For five samples in the nanofluid burnishing process, the values for speed and feed rate were fixed. However, the values for penetration depth and the number of passes were the same as those in the first group. The speed, feed rate values, burnishing length, and maximum depth in each longitudinal tool traverse across the workpiece were selected to be 180 rev/min, 0.11mm/rev, 50 mm, and 0.1 mm, respectively.

### 3- 3- Investigation of surface roughness and microhardness parameters

After the dry and nanofluid burnishing processes, the values for surface roughness and microhardness were investigated. To obtain the surface quality of burnished specimens a portable surface roughness device, model MarSurf TS1, was used. Then, the cut-off length and the arithmetic surface roughness values were assessed in both of the burnishing groups according to the ISO 4288 standard [29]. Each burnished sample was investigated three times to ensure the accuracy of the measurements. Also, four samples with penetration values of 0.2, 0.3, 0.4, and 0.5 mm were chosen to assess Vickers hardness number (HV) values based on ASTM E92 [30]. For each sample, the microhardness value was measured three times in the Falcon 400 machine.

## 4- Results and Discussion

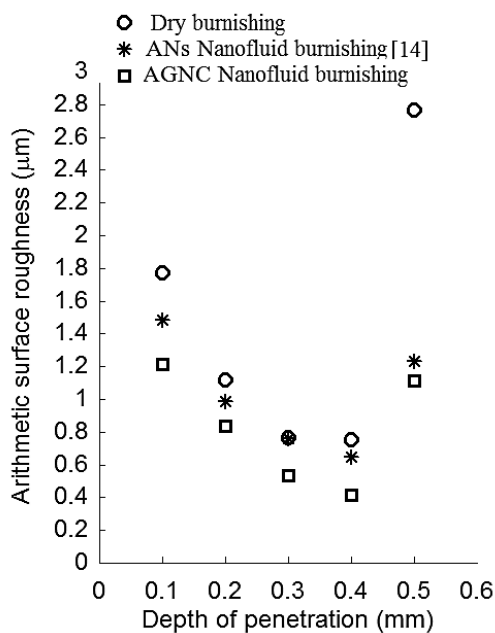
### 4- 1- Effect of burnishing process on surface roughness parameter

The surface roughness values of the aluminum alloy workpieces manufactured through dry and nanofluid burnishing processes are given in Table 3. The penetration depth value of zero in Table 3 is the initial surface quality of Al7175-T74 after the machining process.

Fig. 6 compares the surface roughness values with the depth of penetration in dry burnishing, AGNC, and ANs [14] burnishing processes.

**Table 3. Surface roughness values in dry and AGNC nanofluid burnishing processes**

Penetration depth (mm)	Number of passes	Burnishing method	$R_a(\mu\text{m})$
0	After machining	-----	<b>1.906</b>
0.1	1	dry	<b>1.772</b>
		with nanofluid	<b>1.212</b>
0.2	2 passes: each pass 0.1 mm	dry	<b>1.120</b>
		with nanofluid	<b>0.843</b>
0.3	3 passes: each pass 0.1 mm	dry	<b>0.766</b>
		with nanofluid	<b>0.533</b>
0.4	4 passes: each pass 0.1 mm	dry	<b>0.757</b>
		with nanofluid	<b>0.412</b>
0.5	5 passes: each pass 0.1 mm	dry	<b>2.770</b>
		with nanofluid	<b>1.116</b>

**Fig. 6. Surface roughness versus depth of penetration in dry, AGNC, and ANs burnishing processes**

According to the previous studies performing burnishing process on the surface of metals is, to a certain depth, effective in decreasing surface roughness values; this depends on workpiece material, machining parameters, and the type of burnishing tool. But generally after a while surface quality falls due to material deterioration. Table 3 indicates that by performing burnishing in both dry and AGNC burnishing processes, surface roughness values are continuously decreased until the penetration depth of 0.4 mm. These results

are compared with ANs burnishing process [14] in Fig. 6. For all burnishing processes, the surface roughness value reached its minimum value in the penetration depth of 0.4 mm and thus the best surface quality is obtained. For the penetration depth of 0.5 mm, the surface experienced deterioration, and surely the surface roughness value significantly increased compared to that of the penetration depth of 0.4 mm. In this study, the burnishing feed rate was selected to be the minimum and equal to 0.11 mm/rev. Based on previous studies, as the feed rate of the burnishing tool decreases, because of the long time that the tool is in contact with the surface of specimens, the bearing stress applied to the surface increases, and obtaining high surface quality becomes possible [14, 31]. From Table 3 it becomes apparent that by employing AGNC nanofluid in the penetration depth of 0.5 mm, the arithmetic surface roughness value decreases by almost 1.6 comparing to the dry burnishing process

So, the values obtained for arithmetic surface roughness in dry burnishing are a function of the feed rate and penetration depth values during the burnishing process. As it is shown in the dry burnishing process, with a fixed feed rate and by increasing the number of passes until the penetration depth of 0.4 mm, surface quality improves.

The nanocomposite used in this study is a mixture of spherical alumina and graphene in the form of the flat honeycomb lattice. These were utilized to fill the microscopic valleys on the Al7175-T74 surface which were created due to cold plastic deformation during the burnishing process. It seems that the weak Van Der Waals forces among graphene layers facilitate the rolling motion of the spherical ANs on the surface of Al7175 samples in AGNC burnishing process. This phenomenon increases the possibilities of microscopic valleys filling on the Al7175 burnished surface. It can be seen that the arithmetic surface roughness parameter in AGNC burnished samples is decreased compared to the ANs

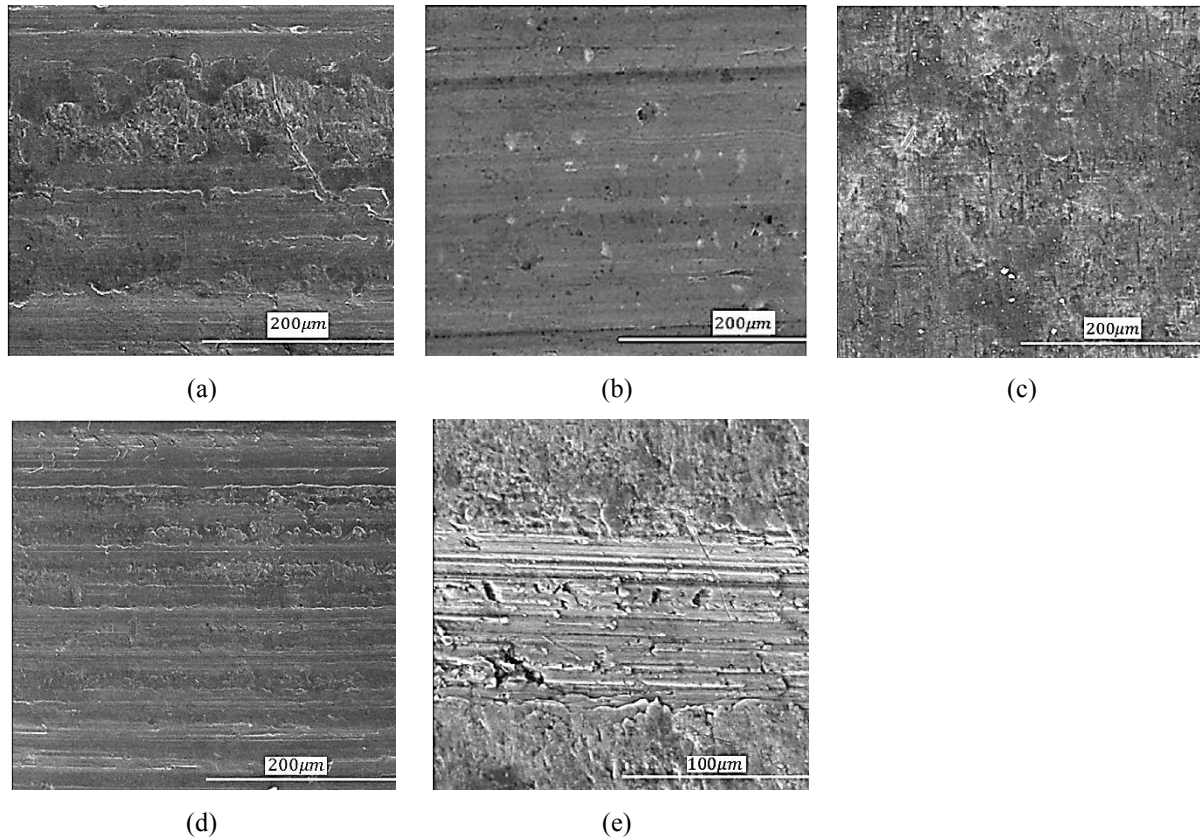


**Fig. 7. SEM Images of the burnished surfaces in AGNC burnishing process at (a) 0.1 mm, (b) 0.2 mm, (c) 0.3 mm, (d) 0.4 mm, and (e) 0.5 mm penetration depth**

burnishing process. In other words, graphene increases the lubrication property among ANs on the surface of burnished samples.

The SEM images from the surface of the AGNC burnished specimens in various depths are presented in Fig. 7. As can be seen in Fig. 7, the surface quality of the aluminum alloy specimens has gradually improved until the penetration depth of 0.4 mm. Fig. 7(e) shows the voids and microcracks in the surface of the burnished specimen at the penetration depth of 0.5 mm which caused surface deterioration. This confirms the material deterioration and its deformation which is a result of the high pressure applied by the burnishing tool. The size of the voids on the surface of the specimens can be easily compared to those of burnishing at the penetration depth of 0.2 mm in Fig. 7(b).

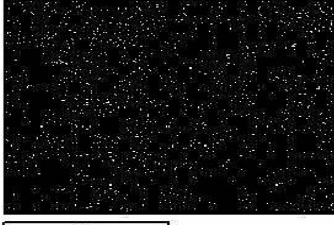
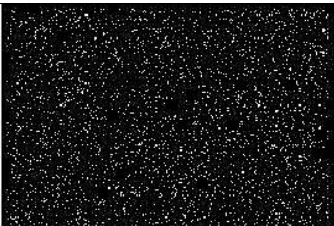
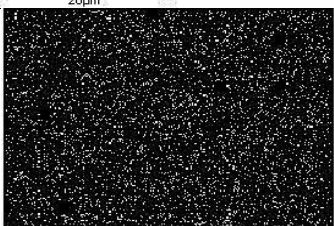
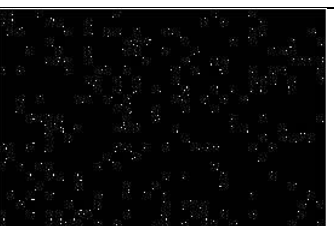
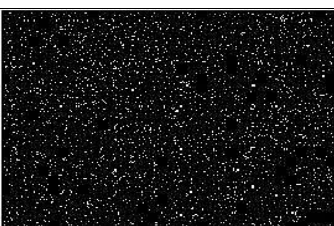
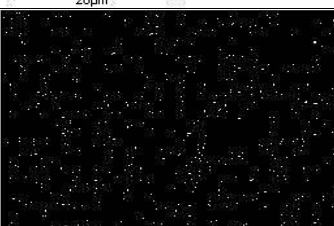
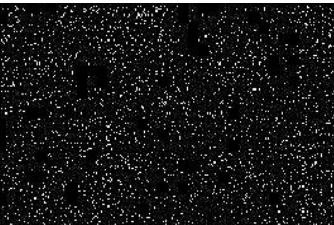
#### 4- 2- Rate of alumina/graphene nanocomposite embedded on aluminum alloy burnished surface in nanofluid burnishing process

In the present study, the EDS analysis of elements distribution is achieved using an EDS connected to an SEM. Moreover, by using the EDS images of the surface of the AGNC burnished Al7175-T74 specimens in various penetration depths; it is possible to specify the distribution of the elements on the surface and to comprehend the presence

of aluminum and oxygen elements in alumina and carbon element in graphene. Since in this research the specimens are made of Al7175-T74, the images of the aluminum element cannot properly reveal the distribution of alumina nanoparticles on the AGNC burnished surfaces. However, to evaluate the distribution of AGNC on the burnished surface, images of carbon and oxygen elements can be employed, respectively. Table 4 depicts the aluminum; oxygen and carbon elements distribution on the surface of AGNC burnished samples.

The images of carbon and oxygen elements remarkably prove that the AGNC embeds on the surface of aluminum alloy samples. Almost in all EDS images the amount of carbon and oxygen elements on the surface increases as the penetration depth is chosen to be higher. Based on previous researches, the presence of graphene on the surface of specimens has a positive effect on their mechanical behavior [32-34]. For instance, when the temperature increases due to wear, the graphene on the surface of metals changes into a sacrificial layer and increases the heat transfer as well as decreasing the temperature on the surface of the workpiece. It can be elicited that the alumina graphene nanocomposite on the surface of the aluminum alloy increases simultaneously the physical and heat transfer properties and can be used in the aluminum shafts, and gears burnishing process for

**Table 4. EDS images of oxygen, carbon, and aluminum distribution on the cylindrical surface of AGNC nanofluid burnished samples**

Penetration depth (mm)	Element		
	Aluminum	Oxygen	Carbon
0.1			
0.2			
0.3			
0.4			
0.5			

**Table 5. The microhardness values of aluminum workpieces burnished by dry and AGNC nanofluid strategies**

Penetration depth (mm)	Number of passes	Burnishing method	Microhardness (HV)
<b>Raw material</b>	-----	-----	148
<b>0.2</b>	2 passes: each pass 0.1 mm	dry	155
		with nanofluid	158
<b>0.3</b>	3 passes: each pass 0.1 mm	dry	164
		with nanofluid	192
<b>0.4</b>	4 passes: each pass 0.1 mm	dry	173
		with nanofluid	215
<b>0.5</b>	5 passes: each pass 0.1 mm	dry	189
		with nanofluid	228

reaching high mechanical and thermal surface strength. It is shown that graphene has attracted great attention worldwide due to its unique combination of mechanical and thermal properties [35, 36]. Thus, graphene is an ideal second phase to improve simultaneously the mechanical, electrical, and thermal properties of metals, ceramics, and polymers [37].

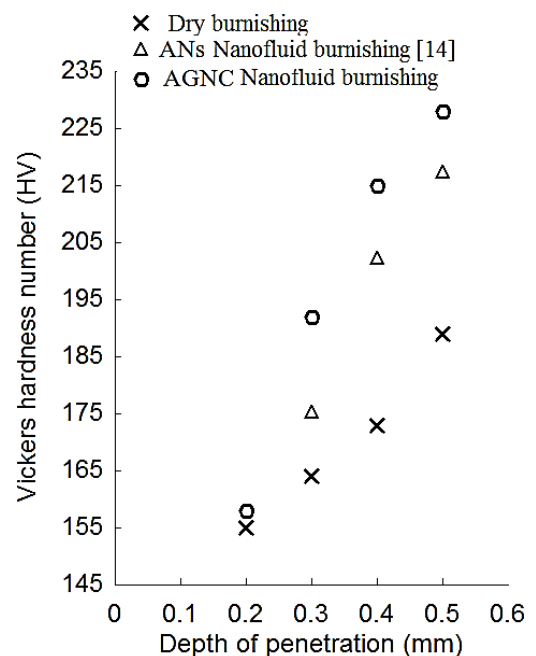
#### 4- 3- Effect of burnishing process on microhardness

To scrutinize the effect of the burnishing process on microhardness of Al7175-T74 specimens, the average initial hardness values of this material were measured before the burnishing process. Four samples of the specimens burnished through dry and AGNC burnishing processes at penetration depths of 0.2, 0.3, 0.4, and 0.5 mm were selected. It should be noted that the similarity of the parameters for both the dry and AGNC burnishing processes makes the comparison of microhardness values easier. The achieved values of microhardness of aluminum alloy workpieces manufactured through dry and AGNC burnishing processes are presented in Table 5.

Fig. 8 reflects the microhardness values in dry, AGNC, and ANs [14] burnishing processes.

Because the burnishing parameters and the tool type are the same, it can be confirmed that the microhardness values for each dry and AGNC burnishing process are a direct function of the penetration depth, the number of burnishing passes, and dry or wet burnishing process. As can be seen in Table 5, the microhardness values are increased by increasing the penetration depth in both burnishing processes. In the burnishing process, the tool pressure along with the cold forming of surface layers increases the microhardness value on the surface. In all cases, the microhardness values obtained from AGNC nanofluid burnishing process are higher than those obtained through the dry burnishing process.

Additionally, by taking into account that feed rate, burnishing tool, and the rotational speed of the machine spindle were selected to be the same for both burnishing

**Fig. 8. Microhardness versus depth of penetration in dry, AGNC, and ANs burnishing processes**

processes it can be proved that one of the reasons for the increase in microhardness values in AGNC nanofluid burnishing process is the AGNC. Transferring AGNC by ethanol alcohol to the burnishing zone along with tool pressure and cold deformation on the material surface traps the nanoparticles on the surface. The EDS images of the AGNC burnished surfaces prove that the amount of oxygen element, as an element of alumina, increases with increasing the penetration depth and at the penetration depth of 0.5 mm reach the maximum level. Therefore, a high amount of

embedded ANs can enhance the microhardness value on the surface of burnished specimens.

Also, the EDS images of the AGNC nanofluid burnished surfaces show that the amount of carbon element increases with increasing the penetration depth up to 0.5 mm. Previous studies confirmed that graphene in  $Al_2O_3$  matrix significantly increases the final hardness of the nanocomposite [23, 26, 27]. According to Fig. 8, the microhardness values obtained from AGNC nanofluid burnishing process are higher than those obtained through the alumina nanofluid burnishing process. In Table 5, the low difference of microhardness values in the penetration depth of 0.2 mm can be due to the limited plastic deformation on the surface of the specimen which traps low AGNC.

## 5- Conclusions

A novel method using nanofluid containing AGNC in the burnishing process was offered. Also, to scrutinize the effects of nanocomposite on the surface characteristics of burnished samples, the results were compared to those obtained from dry and ANs nanofluid burnishing processes. The results can be summarized as follows:

Using dry and AGNC nanofluid burnishing processes in Al7175-T74 specimens continuously decrease arithmetic surface roughness until the penetration depth of 0.4 mm.

By performing dry and AGNC nanofluid burnishing processes in the penetration depth of 0.5 mm the surface of the specimens experience high deterioration and the surface roughness parameter in this case significantly increases compared to the penetration depth of 0.4 mm.

The results showed that the arithmetic surface roughness parameter in AGNC nanofluid burnished samples is decreased by approximately 0.277, 0.233 and 0.345 for the penetration depths of 0.2, 0.3, and 0.4mm compared to those of dry burnishing process.

The results showed that the arithmetic surface roughness parameter in AGNC nanofluid burnished samples is decreased approximately 0.14, 0.231 and 0.235 for the penetration depths of 0.2, 0.3, and 0.4mm compared to those of ANs nanofluid burnishing process.

SEM images showed that the size of voids and cracks increased due to the surface deterioration of Al7175-T74 samples at the penetration depth of 0.5 mm.

The difference in microhardness values enhanced by increasing the penetration depth in both burnishing processes; in all cases, the microhardness values obtained from the nanofluid burnishing process were higher than the dry and alumina burnishing process.

Fig. 8 reflects that the values of microhardness for the AGNC nanofluid burnished samples with four penetration depths of 0.2, 0.3, 0.4, and 0.5 mm are increased about 3 HV, 28 HV, 42 HV, and 39 HV comparing to those values of dry burnishing process.

Fig. 8 reflects that the values of microhardness for the AGNC nanofluid burnished samples with three penetration depths of 0.3, 0.4, and 0.5mm are increased by about 17 HV, 13 HV, and 11 HV comparing to those values of ANs

nanofluid burnishing process.

In dry and AGNC nanofluid burnishing processes of Al7175-T74 samples, minimum surface roughness and high microhardness values can be reached at the penetration depth of 0.4 mm.

The EDS images proved that AGNC has been embedded on the surface of burnished samples.

## References

- [1] M. El-Khabeery, M. El-Axir, Experimental techniques for studying the effects of milling roller-burnishing parameters on surface integrity, *International Journal of machine tools and manufacture*, 41(12) (2001) 1705-1719.
- [2] S. Sattari, A. Atrian, Investigation of deep rolling effects on the fatigue life of Al-SiC nanocomposite, *Materials Research Express*, 5(1) (2018) 015052.
- [3] B. Buldum, S. Cagan, Study of ball burnishing process on the surface roughness and microhardness of AZ91D alloy, *Experimental Techniques*, 42(2) (2018) 233-241.
- [4] H. Luo, J. Liu, L. Wang, Q. Zhong, Investigation of the burnishing process with PCD tool on non-ferrous metals, *The International Journal of Advanced Manufacturing Technology*, 25(5-6) (2005) 454-459.
- [5] D.S. Rao, H.S. Hebbar, M. Komaraiah, U. Kempaiah, Investigations on the effect of ball burnishing parameters on surface hardness and wear resistance of HSLA dual-phase steels, *Materials and Manufacturing processes*, 23(3) (2008) 295-302.
- [6] M.S. John, N. Banerjee, K. Shrivastava, B. Vinayagam, Optimization of roller burnishing process on EN-9 grade alloy steel using response surface methodology, *Journal of the Brazilian Society of Mechanical Sciences and Engineering*, 39(8) (2017) 3089-3101.
- [7] S. Randjelovic, B. Tadic, P.M. Todorovic, D. Vukelic, D. Miloradovic, M. Radenkovic, C. Tsiafis, Modelling of the ball burnishing process with a high-stiffness tool, *The International Journal of Advanced Manufacturing Technology*, 81(9-12) (2015) 1509-1518.
- [8] W.B. Sai, J. Lebrun, Influence of finishing by burnishing on surface characteristics, *Journal of Materials Engineering and Performance*, 12(1) (2003) 37-40.
- [9] B. Sachin, S. Narendranath, D. Chakradhar, Sustainable diamond burnishing of 17-4 PH stainless steel for enhanced surface integrity and product performance by using a novel modified tool, *Materials Research Express*, 6(4) (2019) 046501.
- [10] B. Sachin, S. Narendranath, D. Chakradhar, Effect of working parameters on the surface integrity in cryogenic diamond burnishing of 17-4 PH stainless steel with a novel diamond burnishing tool, *Journal of Manufacturing Processes*, 38 (2019) 564-571.
- [11] S. Ebeid, T. Ei-Taweel, Surface improvement through hybridization of electrochemical turning and roller burnishing based on the Taguchi technique, *Proceedings of the Institution of Mechanical Engineers, Part B: Journal of Engineering Manufacture*, 219(5) (2005) 423-430.
- [12] H. Luo, J. Liu, L. Wang, Q. Zhong, The effect of

- burnishing parameters on burnishing force and surface microhardness, *The International Journal of Advanced Manufacturing Technology*, 28(7-8) (2006) 707-713.
- [13] I. Ozkul, Ball burnishing process effects on surface roughness for Al 6013 alloy, *Turkish Journal of Engineering*, 3(1) (2019) 9.
- [14] S. Khalilpourazary, J. Salehi, How alumina nanoparticles impact surface characteristics of Al7175 in roller burnishing process, *Journal of Manufacturing Processes*, 39 (2019) 1-11.
- [15] S. Khalilpourazary, S. Meshkat, Investigation of the effects of alumina nanoparticles on spur gear surface roughness and hob tool wear in hobbing process, *The International Journal of Advanced Manufacturing Technology*, 71(9-12) (2014) 1599-1610.
- [16] B. Mills, *Machinability of engineering materials*, Springer Science & Business Media, 2012.
- [17] J.G. Kaufman, *Introduction to aluminum alloys and tempers*, ASM international, 2000.
- [18] U.G.-T.M.P. PROCESU, Use of grey based Taguchi method in ball burnishing process for the optimization of surface roughness and microhardness of AA 7075 aluminum alloy, *Materiali in tehnologije*, 44(3) (2010) 129-135.
- [19] S. Said, S. Mikhail, M. Riad, Recent processes for the production of alumina nano-particles, *Materials Science for Energy Technologies*, 3 (2020) 344-363.
- [20] Z. Ma, X. Zhao, Q. Tang, Z. Zhou, Computational prediction of experimentally possible g-C<sub>3</sub>N<sub>3</sub> monolayer as hydrogen purification membrane, *International journal of hydrogen energy*, 39(10) (2014) 5037-5042.
- [21] T. Huang, Y. Xin, T. Li, S. Nutt, C. Su, H. Chen, P. Liu, Z. Lai, Modified graphene/polyimide nanocomposites: reinforcing and tribological effects, *ACS applied materials & interfaces*, 5(11) (2013) 4878-4891.
- [22] J. Wang, Z. Li, G. Fan, H. Pan, Z. Chen, D. Zhang, Reinforcement with graphene nanosheets in aluminum matrix composites, *Scripta Materialia*, 66(8) (2012) 594-597.
- [23] R. Jiang, H. Zhu, Y. Fu, S. Jiang, E. Zong, J. Yao, Photocatalytic decolorization of Congo red wastewater by magnetic ZnFe<sub>2</sub>O<sub>4</sub>/graphene nanosheets composite under simulated solar light irradiation, *Ozone: Science & Engineering*, 42(2) (2020) 174-182.
- [24] N.N.M. Zorkipli, N.H.M. Kaus, A.A. Mohamad, Synthesis of NiO nanoparticles through sol-gel method, *Procedia chemistry*, 19 (2016) 626-631.
- [25] S. Pourmand, M. Abdouss, A. Rashidi, Preparation of nanoporous graphene via nanoporous zinc oxide and its application as a nanoadsorbent for benzene, toluene and xylenes removal, *International Journal of Environmental Research*, 9(4) (2015) 1269-1276.
- [26] E. Klyatskina, A. Borrell, E. Grigoriev, A. Zholnin, M. Salvador, V. Stolyarov, Structure features and properties of graphene/Al<sub>2</sub>O<sub>3</sub> composite, *J. Ceram. Sci. Technol*, 9 (2018) 215-224.
- [27] X. Liu, Y.C. Fan, Q. Feng, L.J. Wang, W. Jiang, Preparation of graphene nanosheet/alumina composites, in: *Materials Science Forum*, Trans Tech Publ, 2013, pp. 534-538.
- [28] A.K. Sharma, A.K. Tiwari, A.R. Dixit, Progress of nanofluid application in machining: a review, *Materials and Manufacturing Processes*, 30(7) (2015) 813-828.
- [29] D.E. ISO, *Geometrical Product Specifications (GPS)—Surface Texture: Profile Method: Rules and Procedures for the Assessment of Surface Texture*, (1996).
- [30] E. ASTM, 92: 2003: *Standard Test Method for Vickers Hardness of Metallic Materials*, ASTM International, (2006).
- [31] J. Maximov, A. Anchev, G. Duncheva, N. Ganev, K. Selimov, Influence of the process parameters on the surface roughness, micro-hardness, and residual stresses in slide burnishing of high-strength aluminum alloys, *Journal of the Brazilian Society of Mechanical Sciences and Engineering*, 39(8) (2017) 3067-3078.
- [32] A.D. Moghadam, E. Omrani, P.L. Menezes, P.K. Rohatgi, Mechanical and tribological properties of self-lubricating metal matrix nanocomposites reinforced by carbon nanotubes (CNTs) and graphene—a review, *Composites Part B: Engineering*, 77 (2015) 402-420.
- [33] L.-Y. Lin, D.-E. Kim, W.-K. Kim, S.-C. Jun, Friction and wear characteristics of multi-layer graphene films investigated by atomic force microscopy, *Surface and Coatings Technology*, 205(20) (2011) 4864-4869.
- [34] S.F. Bartolucci, J. Paras, M.A. Rafiee, J. Rafiee, S. Lee, D. Kapoor, N. Koratkar, Graphene–aluminum nanocomposites, *Materials Science and Engineering: A*, 528(27) (2011) 7933-7937.
- [35] A.A. Balandin, S. Ghosh, W. Bao, I. Calizo, D. Teweldebrhan, F. Miao, C.N. Lau, Superior thermal conductivity of single-layer graphene, *Nano letters*, 8(3) (2008) 902-907.
- [36] L.S. Walker, V.R. Marotto, M.A. Rafiee, N. Koratkar, E.L. Corral, Toughening in graphene ceramic composites, *ACS nano*, 5(4) (2011) 3182-3190.
- [37] M. Liu, C. Chen, J. Hu, X. Wu, X. Wang, Synthesis of magnetite/graphene oxide composite and application for cobalt (II) removal, *The Journal of Physical Chemistry C*, 115(51) (2011) 25234-25240.

#### HOW TO CITE THIS ARTICLE

S. M. Hadad Baygi. A hybrid optimal-base fuzzy-proportional-integral-derivative controller for vibration mitigation of structural system against earthquake. *AUT J. Mech Eng.*, 5(2) (2021) 255-264.

DOI: 10.22060/ajme.2020.17420.5861

